CAROSI, G., and CHANSON, H. (2007). "Self-Similarity of Air-Water Flows in Skimming Flows on Stepped Spillways." *Proc. 32nd IAHR Biennial Congress*, Venice, Italy, G. DI SILVIO and S LANZONI Editors, Topic C2.b, 10 pages (CD-ROM).

SELF-SIMILARITY OF AIR-WATER FLOWS IN SKIMMING FLOWS ON STEPPED SPILLWAYS

Giovanna CAROSI and Hubert CHANSON
Div of Civil Engineering, The University of Queensland, Brisbane QLD 4072, Australia
Ph.: (61 7) 3365 4163 - Fax: (61 7) 3365 4599 - E-mail: h.chanson@uq.edu.au

Abstract : Skimming flows on stepped spillways are characterised by a significant rate of turbulent dissipation on the chute. Herein an advanced signal processing of traditional conductivity probe signals is developed to provide further details on the turbulent time and length scales. The technique is applied to a 22° stepped chute operating with flow Reynolds numbers between 3.8 and 7.1 E+5. The new correlation analyses yielded a characterisation of large eddies advecting the bubbles. The turbulent length scales were related to the characteristic depth Y_{90}. Some self-similar relationships were observed systematically at both macroscopic and microscopic levels. These included the distributions of void fraction, bubble count rate, interfacial velocity and turbulence level, and turbulence time and length scales. The self-similarity results were significant because they provided a picture general enough to be used to characterise the air-water flow field in prototype spillways.
Keywords : Stepped spillways, Skimming flows, Air-water flow properties, Self-similarity, Turbulent length and time scales, Signal processing.

INTRODUCTION

Stepped spillways have been used for many centuries. The stepped design increases the rate of energy dissipation on the chute and reduces the size of the downstream energy dissipation system (Fig. 1). For the last fifteen years, the research in the hydraulics of stepped spillways has been active (e.g. CHANSON 2001). On a stepped spillway, the waters flow as a succession of free-falling nappes (nappe flow regime) at small discharges (TOOMBES 2002). For a range of intermediate flow rates, a transition flow regime is observed (CHANSON and TOOMBES 2004). Modern stepped spillways are typically designed for large discharge capacities corresponding to a skimming flow regime (RAJARATNAM 1990). In a skimming flow, the flow is non-aerated at the upstream end of the chute. Free-surface aeration occurs when the turbulent shear next to the free-surface becomes larger than the bubble resistance offered by surface tension and buoyancy. Downstream of the inception point of free-surface aeration, some strong air-water mixing takes place. Large amounts of air are entrained, and very-strong interactions between main stream turbulence, step cavity recirculation zones and free-surface are observed associated with strong energy dissipation and flow resistance (CHANSON and TOOMBES 2002).

It is the purpose of this study to investigate thoroughly the air-water flow properties in skimming flows, with a focus on the turbulent characteristics and self-similarity. New measurements were conducted in a large-size facility ($\theta = 22^o$, $h = 0.1$ m) using simultaneously several phase-detection intrusive probes. Detailed air-water flow properties were recorded systematically for several flow rates. The results included the distributions of turbulence intensity and of integral turbulent scales.

DIMENSIONAL ANALYSIS AND SIMILITUDE

A key feature of skimming flows on a stepped chute is the strong free-surface aeration and air-water flow turbulence. In a dimensional analysis, the relevant parameters must include the fluid properties and physical constants, the chute geometry and inflow conditions, the air-water turbulent flow properties and the geometry of the steps. Considering a skimming flow at uniform equilibrium down a stepped chute with flat horizontal steps and for a prismatic rectangular channel, a thorough dimensional analysis yields a relationship between the local air-water flow properties, and the fluid properties, physical constants, flow conditions and step geometry (e.g. CHANSON 2004, CAROSI and CHANSON 2006). When the chute slope θ, the step height h, the channel width W and the step roughness are constant, it yields:

$$C, \frac{V}{\sqrt{g * d_c}}, \frac{u'}{V}, T \times \sqrt{\frac{g}{d_c}}, \frac{L_{xy}}{d_c} = F\left(\frac{x}{d_c}, \frac{y}{d_c}, \frac{d_c}{h}, Re\right) \quad (1)$$

where C is the local void fraction, V is the local velocity, g is the gravity acceleration, d_c is the critical depth, u' is a characteristic turbulent velocity, T is a turbulent time scale, L_{xy} is a turbulent length scale, x and y is the longitudinal and normal coordinates, and Re is the Reynolds number. Equation (1) gives a dimensionless expression of the local air-water turbulent flow properties as functions of independent parameters that include both Froude and Reynolds numbers.

The validity of the Froude similitude itself was rarely tested in stepped chutes but in a few studies (CHANSON 2004). Recent studies of air-water flow properties yielded stringent conditions to minimise scale effects suggesting the impossibility to achieve true dynamic similarity even in large-size models (BOES 2000, CHANSON and GONZALEZ 2005).

Fig. 1 - Photograph of Pedrogao dam stepped spillway, Portugal on 4 Sept. 2006 - RCC gravity dam completed in March 2006, uncontrolled stepped spillway (h = 0.6 m, 1V:0.75H)

EXPERIMENTAL APPARATUS AND PROCEDURES

New experiments were performed at the University of Queensland (Table 1). The experimental channel was previously used by CHANSON and TOOMBES (2002) and GONZALEZ (2005). Waters were supplied from a large feeding basin leading to a sidewall convergent with a 4.8:1 contraction ratio. The test section consisted of a broad-crested weir (1 m wide, 0.6 m long) followed by ten identical steps (h = 0.1 m, l = 0.25 m) made of marine ply. The stepped chute was 1 m wide with perspex sidewalls followed by a horizontal concrete canal ending in a dissipation pit. The pump delivering the flow rate was controlled with an adjustable frequency AC motor drive which enabled an accurate discharge adjustment in the closed-circuit system. Further details on the experiments were reported in CAROSI and CHANSON (2006).

Clear-water flow depths were measured with a point gauge. The water discharge was measured from the upstream head above the crest, and the head-discharge relationship was checked with detailed velocity distribution measurements on the crest itself. Air-water flow properties were measured with single-tip and double-tip conductivity probes. Basic air-water flow measurements were performed with single-tip conductivity probes (∅ = 0.35 mm). Additional measurements were performed with a dual-tip conductivity probe (∅ = 0.25 mm, Δx = 7.0 mm). All the probes were excited by an electronic system (Ref. UQ82.518) designed with a response time less than 10 μs and calibrated with a square wave generator. The probe sensors were scanned at 20 kHz per sensor for 45 seconds for all experiments.

Table 1 - Summary of experimental flow conditions on the stepped chute

Ref.	θ	h	Q_w	Re	Instrumentation
	deg.	m	m^3/s		
(1)	(2)	(3)	(4)	(5)	(6)
CHANSON and TOOMBES (2002)	15.9	0.1	0.07 to 0.18	2.7 to 7.5 E+5	Dual-tip probe
	21.8	0.1	0.06 to 0.18	2.3 to 7.3 E+3	(Ø = 0.025 mm, Δx = 8 mm).
GONZALEZ (2005)	15.9	0.05	0.02 to 0.2	0.79 to 8 E+5	Dual-tip probe
	15.9	0.1	0.08 to 0.2	3.2 to 8 E+5	(Ø = 0.025 mm, Δx = 8 mm).
	21.8	0.1	0.09 to 0.18	3.8 to 7.1 E+5	
Present study	21.8	0.1	0.09 to 0.18	3.8 to 7.1 E+5	Single-tip probes (Ø = 0.35 mm). Separation distance: z = 3.6 to 55.7 mm.
					Dual-tip probe (Ø = 0.25 mm, Δx = 7.0 mm).

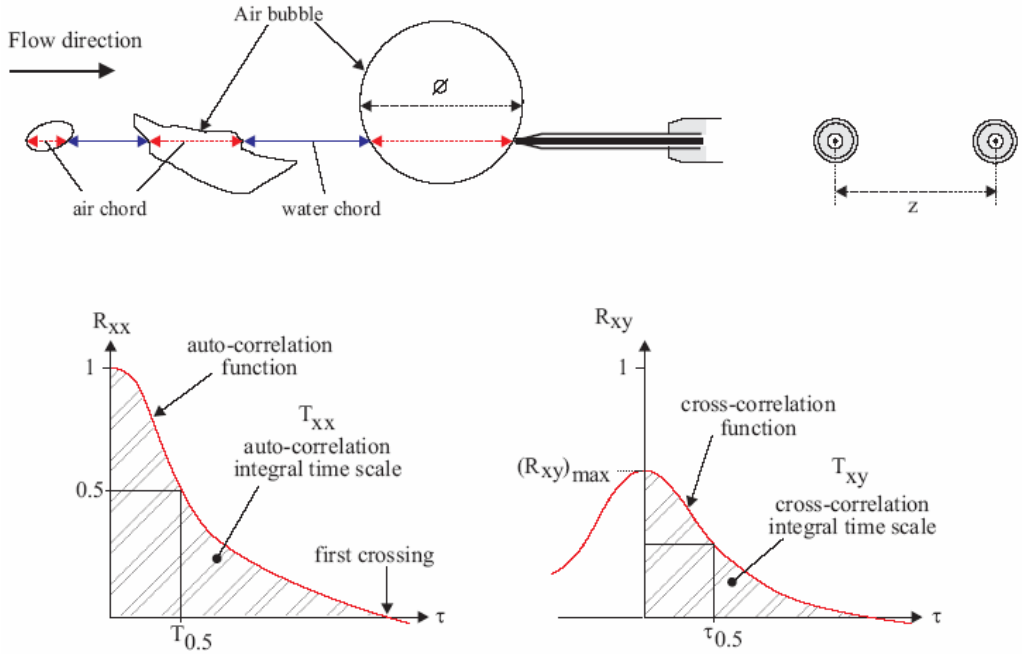

Fig. 2 - Definition sketch of two single-tip conductivity probes side-by-side and of the auto- and cross-correlation functions

CORRELATION ANALYSIS

The interfacial velocities V were deduced from a cross-correlation analysis between the sensors of the double-tip probe. The turbulence intensities (Tu = u'/V) were derived from the relative width of the cross-correlation function (CHANSON and TOOMBES 2002).

With the single-tip probe, all measurements were conducted on the channel centreline (z = 0), and a second identical probe was placed beside the first one with the probe sensors at the same vertical and streamwise distances y and x respectively, but separated by a known transverse distance z (Fig. 2). Their signals was analysed in terms of auto-correlation and cross-correlation functions R_{xx} and R_{xy} respectively. Following CHANSON (2006), the correlation analysis results included the maximum cross-correlation coefficient $(R_{xy})_{max}$, and the correlation time scales T_{xx} and T_{xy} (Fig. 2). The integral time scale T_{xx} represents an integral time scale of the longitudinal bubbly flow structure. When identical experiments are repeated with different separation distances z, some integral turbulent length and time scales may be calculated as :

$$L_{xy} = \int_{z=0}^{z=z((R_{xy})_{max}=0)} (R_{xy})_{max} \times dz \qquad (2)$$

$$T = \left(\int_{z=0}^{z=z((R_{xy})_{max}=0)} (R_{xy})_{max} \times T_{xy} \times dz \right) / L_{xy} \quad (3)$$

Herein, experiments were repeated with z = 3.6 to 56 mm, while the data for z = 0 were deduced from the auto-correlation analysis.

EXPERIMENTAL RESULTS

BASIC FLOW PATTERNS

The basic flow regimes were inspected in a series of preliminary experiments with discharges ranging from 0.008 to 0.180 m^3/s. For small flow rates ($d_C/h < 0.5$), the waters flowed as a succession of free-falling jets that was typical of a nappe flow regime. For some intermediate discharges ($0.5 < d_C/h < 0.95$), the flow had a chaotic behaviour characterised by strong splashing and droplet projections downstream of the inception point of free-surface aeration. For larger flows ($d_C/h > 0.95$), the waters skimmed above the pseudo-bottom formed by the step edges. The skimming flows were characterised by strong cavity recirculation with three-dimensional vortical patterns. These were best seen next to the inception point of free-surface aeration. Overall the results in terms of flow regimes were very close to the earlier observations of CHANSON and TOOMBES (2002) and GONZALEZ (2005).

DISTRIBUTIONS OF VOID FRACTION AND BUBBLE COUNT RATE

Experimental observations demonstrated some substantial free-surface aeration immediately downstream of the inception point of free-surface aeration while the flow aeration was sustained further downstream. This is illustrated in Figure 3 where the dimensionless distributions for void fraction C and bubble count rate $F \times d_C/V_C$ are presented as functions of y/Y_{90} for several successive step edges for the same flow rate, where y is the distance normal to the pseudo-bottom formed by the step edges, Y_{90} is the characteristic distance where C = 0.90, and d_C and V_C are respectively the critical flow depth and velocity. For the data shown in Figure 3, the flow aeration was nil at step edge 7 immediately upstream of the inception point. Between step edges 7 and 8, some strong self-aeration took place. The amount of entrained air and the mean air content were about constant between step edges 8 and 10, and the depth-averaged void fraction C_{mean} was 0.32 in average.

The void fraction profiles showed consistently a similar shape (Fig. 3). The dimensionless distributions exhibited a S-shape profile that was observed in previous skimming flow studies: e.g., RUFF and FRIZELL (1994), CHANSON and TOOMBES (1997,2002). For all the data, the void fraction distribution measurements compared well with an analytical solution of the advective diffusion equation for air bubbles :

$$C = 1 - \tanh^2\left(K' - \frac{y'}{2 \times D_o} + \frac{(y'-1/3)^3}{3 \times D_o} \right) \quad (4)$$

where $y' = y/Y_{90}$, K' is an integration constant and D_o is a function of the depth-averaged void fraction C_{mean} only :

$$K' = 0.3274 + \frac{1}{2 \times D_o} - \frac{8}{81 \times D_o} \quad (5)$$

$$C_{mean} = 0.762 \times (1.043 - \exp(-3.614 \times D_o)) \quad (6)$$

Equation (4) was first developed by CHANSON and TOOMBES (2002) and it is compared with some dimensionless void fraction data in Figure 3.

The dimensionless distributions of bubble count rate showed consistently a characteristic shape with a maximum value observed for void fractions between 40 and 60% (Fig. 3). A similar result was observed in smooth chute and stepped spillway flows (e.g. CHANSON 1997b, CHANSON and TOOMBES 2002, TOOMBES 2002, GONZALEZ 2005). The relationship between bubble frequency

and void fraction was approximately a parabolic shape :

$$F / F_{max} = 4 \times C \times (1 - C) \quad (7)$$

In the present study, the maximum bubble count rate F_{max} was observed for $0.4 \leq C \leq 0.5$ (Fig. 3). TOOMBES (2002) demonstrated some theoretical validity of Equation (7) and he extended the reasoning to further air-water flow situations.

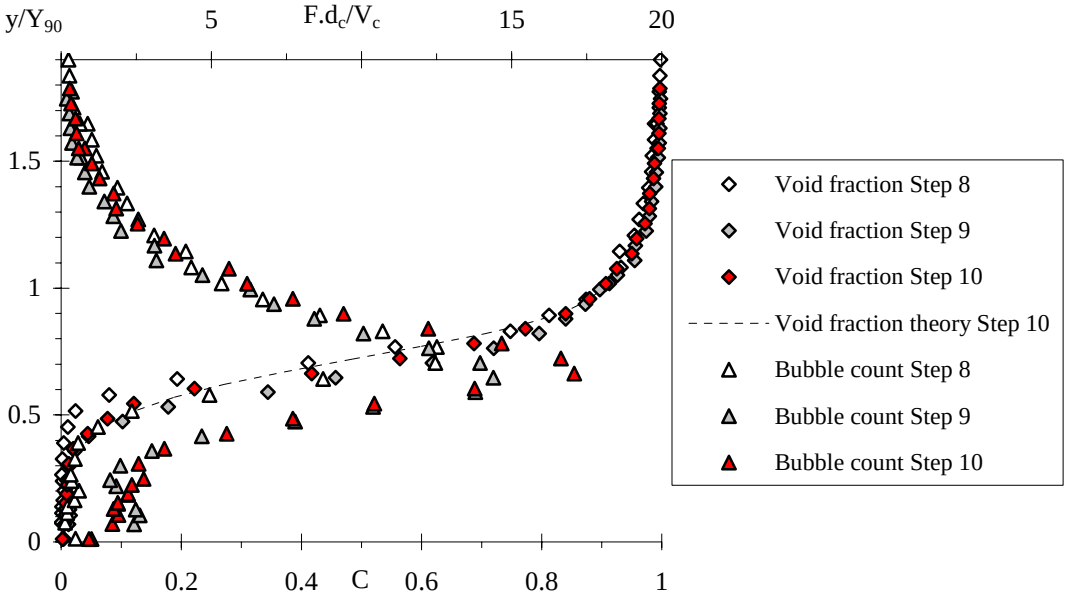

Fig. 3 - Dimensionless distributions of void fraction and bubble count rate: comparison between Equation (4) and void fraction data for $d_C/h = 1.57$ (single-tip probe data)

DISTRIBUTIONS OF INTERFACIAL VELOCITY AND TURBULENCE LEVEL

At each step edge, the time-averaged velocity and turbulent velocity fluctuation profiles showed some characteristic shapes (Fig. 4). The interfacial velocity distributions presented a smooth shape similar to earlier results on stepped chutes (e.g. BOES 2000, CHANSON and TOOMBES 2002, GONZALEZ 2005). Importantly, the velocity distributions showed some self-similarity. All the data followed closely a power-law function for $y/Y_{90} \leq 1$. For $y/Y_{90} > 1$, the velocity profile was quasi-uniform. That is :

$$V / V_{90} = y'^{1/N} \qquad 0 \leq y' \leq 1 \quad (8)$$

$$V / V_{90} = 1 \qquad 1 \leq y' \quad (9)$$

where V_{90} is the characteristic air-water velocity at $y = Y_{90}$. Several researchers observed the velocity profile described by Equation (8), but few studies documented the velocity distribution in the upper spray region (GONZALEZ 2005). Present data are compared with Equations (8) and (9) in Figure 4. For the present experiments, the exponent N was about 10, although it varied between a step edge and the next consecutive step edge for a given flow rate. The variations were believed to reflect some flow interactions between adjacent shear layers and cavity flows.

The turbulent intensity profiles exhibited some maximum turbulence level for $0.3 \leq y/d_C \leq 0.4$ which corresponded to about $C \approx 0.4$ to 0.6 (Fig. 4). The experimental data showed a strong correlation between the turbulence intensity Tu and the bubble count rate F, and all the data collapsed reasonably well into a single curve :

$$Tu = 0.25 + 0.035 \times (F \times d_C / V_C)^{1.2} \quad (10)$$

Equation (10) reflects a monotonic increase in turbulence level with an increasing bubble count rate. The limit for F = 0 (i.e. Tu = 0.25) is close to monophase flow measurements on a stepped chute upstream of the inception point of free-surface aeration (OHTSU and YASUDA 1997, AMADOR et al. 2004). It is hypothesised that the large number of air-water interfaces, and the continuous deformations of the air-water interfacial structure generated large turbulence levels measured by the intrusive phase-detection probe.

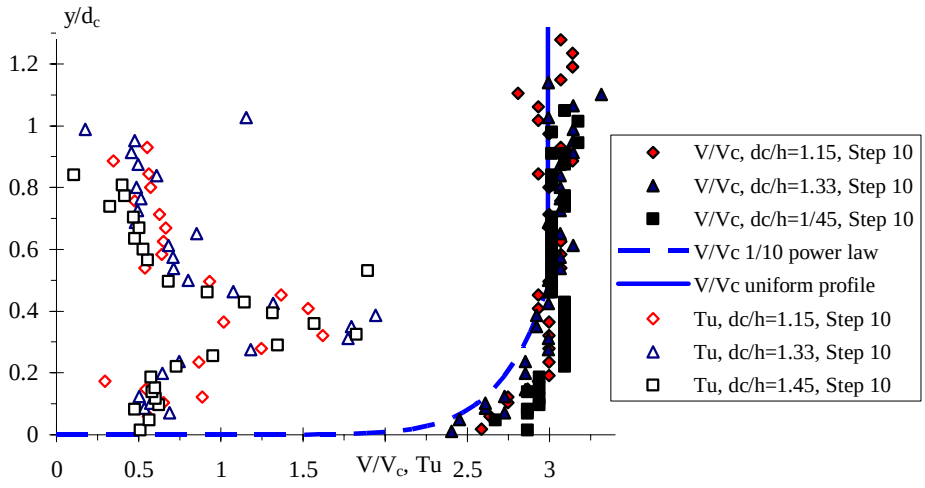

Fig. 4 - Dimensionless distributions of velocity V/V_C and turbulence intensity Tu for d_C/h = 1.15, 1.33 and 1.45 at step edge 10

CORRELATION FUNCTIONS AND TIME SCALES

The correlation functions exhibited similar patterns for all investigated flow conditions. The auto-correlation functions were best fitted by :

$$R_{xx} = 1/\left(1+(\tau/T_{0.5})^{1.3}\right) \quad (11)$$

where τ is the time lag and $T_{0.5}$ is the time lag for which R_{xx} = 0.5 (Fig. 2). The cross-correlation functions exhibited clearly a marked maximum $(R_{xy})_{max}$ which decreased with increasing sensor separation z. They followed closely a Gaussian error function :

$$\frac{R_{xy}}{(R_{xy})_{max}} = \exp\left(-\frac{1}{1443}\times\frac{\tau^2}{\tau_{0.5}}\right) \quad (12)$$

where $(R_{xy})_{max}$ is the maximum normalised cross-correlation value, and $\tau_{0.5}$ is the time lag for which $R_{xy} = 0.5\times(R_{xy})_{max}$ (Fig. 2). The finding (Eq. (12)) was observed systematically at all sampling locations for $\tau/\tau_{0.5} < 2$.

The distributions of correlation time scales T_{xx} and T_{xy} exhibited a typical relationship between void fraction and correlation time scales at a given flow cross-section. Both the distributions of auto- and cross-correlation time scales T_{xx} and T_{xy} presented a parabolic shape for $0 \le C \le 0.95$ at all step edges and for all investigated flow rates:

$$T_{xy}/(T_{xy})_{max} = 4\times C\times(1-C) \quad (13)$$

where $(T_{xy})_{max}$ is the maximum cross-correlation time scale in the cross-section for a given separation distance z.

TURBULENT TIME AND LENGTH SCALES

The turbulent length and time scales, L_{xy} and T respectively, were calculated using Equations (2) and (3) based upon correlation analyses conducted with several transverse separation distances.

Typical results in terms of the dimensionless turbulent length scale L_{xy}/Y_{90}, and time scale $T \times \sqrt{g / Y_{90}}$ are presented in Figure 5. The measured void fraction data are also shown in Figure 5.

The turbulent length scale L_{xy} represents a characteristic dimension of the large vortical structures advecting the air bubbles and air-water packets. In bubbly flows, the turbulent length scales are closely linked with the characteristic sizes of the large-size eddies and their interactions with entrained air bubbles. This was evidenced by high-speed photographs demonstrating air bubble trapping in large eddies of developing mixing layers (e.g. HOYT and SELLIN 1989, CHANSON 1997a). Herein the integral turbulent length scale L_{xy} represented a measure of the size of large vortical structures advecting air bubbles in the skimming flow regime. The air-water turbulent length scale was closely related to the characteristic air-water depth Y_{90} : i.e., $0.05 \leq L_{xy}/Y_{90} \leq 0.2$. This result was irrespective of the flow Reynolds numbers within the range of the experiments. The turbulence time scale T characterises the integral turbulent time scale of the large eddies advecting the air bubbles and air-water particle clusters. The integral turbulent time scales were typically $0.01 \leq T \times \sqrt{g / Y_{90}} \leq 0.06$ (Fig. 8).

The relationships between the integral length scales L_{xy} and integral time scale T, and the void fraction exhibited a "skewed parabolic shape" with maxima occurring for void fractions between 0.6 and 0.7 (CAROSI and CHANSON 2006). The dimensionless distributions of transverse turbulent length scale L_{xy}/Y_{90}, and of transverse integral turbulent time scale $T \times \sqrt{g / Y_{90}}$ were best correlated by :

$$L_{xy} / (L_{xy})_{max} = 1.75 \times C^{0.57} \times (1 - C)^{0.32} \qquad 0 \leq C \leq 1 \quad (14)$$

$$T / T_{max} = 1.97 \times C^{0.59} \times (1 - C)^{0.50} \qquad 0 \leq C < 0.97 \quad (15)$$

where $(L_{xy})_{max}$ and T_{max} are the characteristic maxima in the cross-section.

The high-velocity open channel flows on the stepped channel were highly turbulent (Fig. 4). Present results demonstrated that the high levels of turbulence were associated directly with some large scale turbulence. In particular, the intermediate region ($0.3 < C < 0.7$) between bubbly and spray regions seemed to play a major role in the development the large vortices and turbulent dissipation. Turbulence level maxima were observed consistently for $0.4 < C < 0.5$, while maximum integral turbulent scales were seen for $0.6 < C < 0.7$. The present findings imply that, while the stepped invert contributes to intense turbulence production, some turbulent energy is dissipated in the form of large-scale vortices in the bulk of the flow.

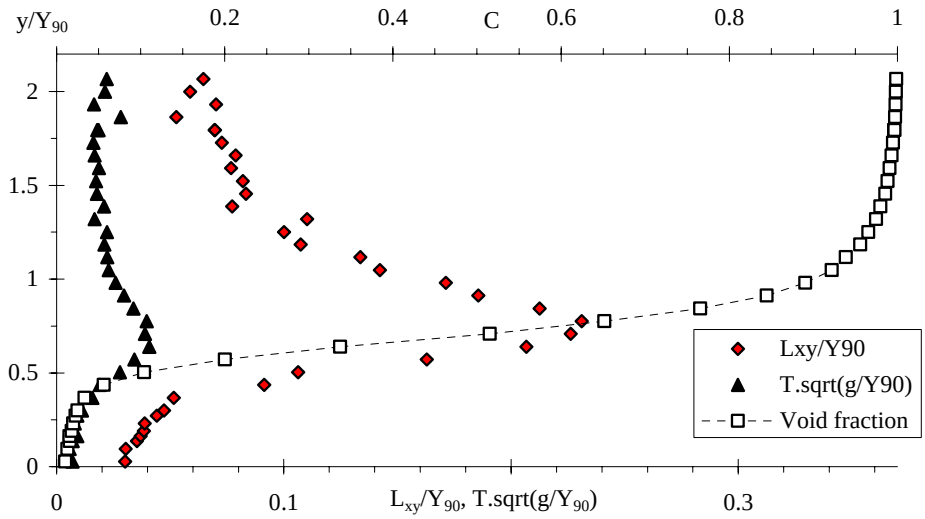

Fig. 5 - Dimensionless distributions of air-water transverse turbulent length scales L_{xy}/Y_{90}, and transverse integral turbulent time scale $T \times \sqrt{g / Y_{90}}$ - $d_c/h = 1.45$, Step edge 10

DISCUSSION : SELF-SIMILARITY IN AIR-WATER FLOW PROPERTIES

A self-similar process is one whose spatial distribution of properties at various times can be obtained from one another by a similarity transformation (BARENBLATT 1996). Self-similarity is a powerful tool in turbulence flow research, and skimming flows on a stepped chute are one type of turbulent flows involving a wide spectrum of spatial and temporal scales. The non-linear interactions among vortices and particles at different scales lead to a complicated flow structure, and relationships among flows at different scales are of crucial significance. These play also a major role in comparing analytical, experimental and numerical results as these results are for different scales. For example, most stepped spillway applications are for prototype flow conditions characterised by very-large flow Reynolds numbers, between 1 E+6 and more than 1 E+9, that cannot be modelled numerically nor physically.

In the present study, self-similarity was observed in terms of the distributions of air-water flow properties. Equations (4), and (7) to (15), demonstrate some basic self-similarity equations that were observed during the present work. Self-similarity is illustrated also in Figures 3, 4 and 6 (also CAROSI and CHANSON 2006). These self-similar relationships were observed at both macroscopic and microscopic levels. For example, the distributions of void fraction and interfacial velocity at a macroscopic level, and the cross-correlation functions and probability distribution functions of bubble chords at a microscopic level.

Self-similarity is closely linked with dynamic similarity. Some researchers argued that it is nearly impossible to achieve a true dynamic similarity in stepped spillway models because of number of relevant dimensionless parameters (Eq. (1)). However the present findings showed a number of self-similar relationships that remain invariant under changes of scale : i.e., they have scaling symmetry which led in turn to remarkable application at prototype scales. Clearly the present results are most significant. They provide a picture general enough to be used, as a first approximation, to characterise the air-water flow field in similar stepped spillway structures irrespective of the physical scale.

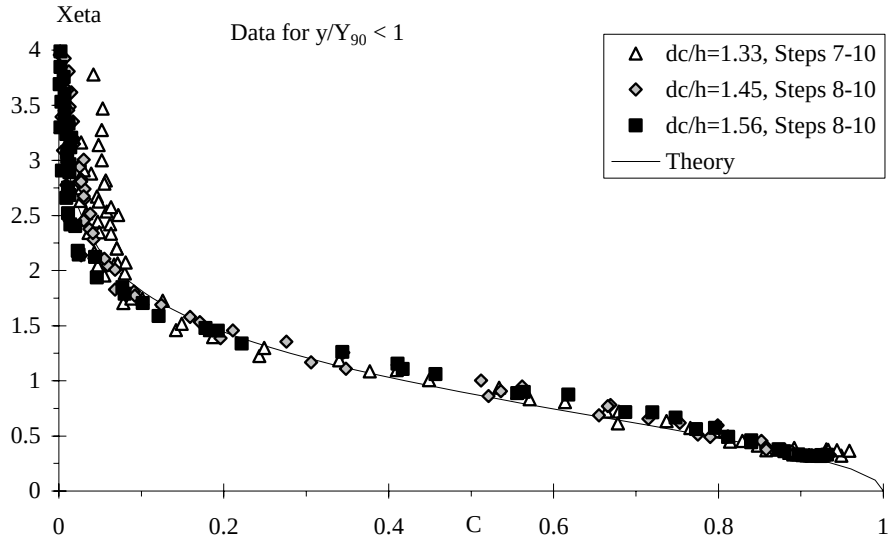

(A) Void fraction distributions: $C = 1 - \tanh^2\chi$ with $\chi = K'-y'/(2\times D_o)+(y'-1/3)^3/(3\times D_o)$ (Eq. (4))

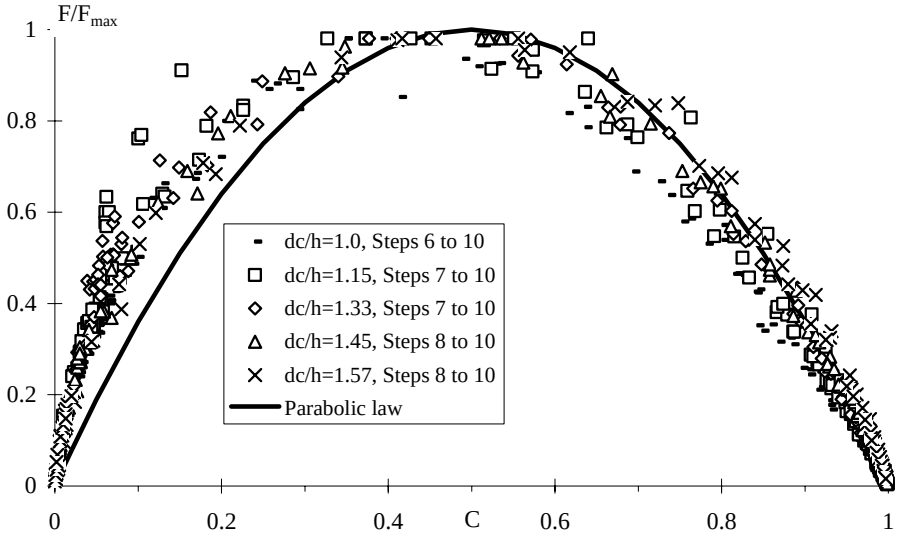

(B) Dimensionless bubble count rate distributions (Eq. (7))

Fig. 6 - Self-similarity in air-water skimming flows on a stepped chute

CONCLUSION

Detailed air-water flow measurements were performed in skimming flows above a stepped chute. The experiments were conducted with flow Reynolds numbers ranging from 3.8 to 7.1 E+5, and measurements were performed with several phase-detection intrusive probes. An advanced signal processing technique with new signal correlation analyses was developed and applied systematically.

The air water flow properties presented some basic characteristics that were qualitatively and quantitatively similar to previous studies in skimming flows. These included the distributions of void fraction, bubble count rate and interfacial velocity. The correlation analyses yielded a characterisation of the large eddies advecting the bubbles. Basic results included the integral turbulent length and time scales. The turbulent length scales characterised some measure of the size of large vortical structures advecting air bubbles in the skimming flows, and the data were closely related to the characteristic air-water depth Y_{90} : i.e., $L_{xy}/Y_{90} \approx 0.05$ to 0.2. The dimensionless integral turbulent time scales were within $0.01 \leq T \times \sqrt{g / Y_{90}} \leq 0.06$. The results were irrespective of the Reynolds numbers within the range of the experiments.

Some self-similar relationships were observed systematically at both macroscopic and microscopic levels. These included the distributions of void fraction, bubble count rate, interfacial velocity and turbulence level at a macroscopic scale, and the bubble chord distributions and auto- and cross-correlation functions at the microscopic level. The experimental results showed a number of self-similar relationships that remained invariant under changes of scale. The present findings are significant because they provide a picture general enough to characterise the air-water flow field in prototype stepped spillways.

REFERENCES

AMADOR, A., SANCHEZ-JUNY, M., DOLZ, J., SANCHEZ-TEMBLEQUE, F., and PUERTAS, J. (2004). "Velocity and Pressure Measurements in Skimming Flow in Stepped Spillways." *Proc. Intl Conf. on Hyd. of Dams & River Structures*, Tehran, Iran, Balkema Publ., pp. 279-285.

BARENBLATT, G.I. (1996). "Scaling, Self-Similarity, and Intermediate Asymptotics." *Cambridge University Press*, UK, 386 pages.

BOES, R.M. (2000). "Scale Effects in Modelling Two-Phase Stepped Spillway Flow." *Intl Workshop on Hydraulics of Stepped Spillways*, Zürich, Switzerland, Balkema Publ., pp. 53-60.

CAROSI, G., and CHANSON, H. (2006). "Air-Water Time and Length Scales in Skimming Flows on a Stepped Spillway. Application to the Spray Characterisation." *Report No. CH59/06*, Div. of Civil Engineering, The University of Queensland, Brisbane, Australia, July, 142 pages.

CHANSON, H. (1997a). "Air Bubble Entrainment in Free-Surface Turbulent Shear Flows." *Academic Press*, London, UK, 401 pages.
CHANSON, H. (1997b). "Air Bubble Entrainment in Open Channels. Flow Structure and Bubble Size Distributions." *Intl Jl of Multiphase Flow*, Vol. 23, No. 1, pp. 193-203.
CHANSON, H. (2001). "The Hydraulics of Stepped Chutes and Spillways." *Balkema*, Lisse, The Netherlands, 418 pages.
CHANSON, H. (2004). "Environmental Hydraulics of Open Channel Flows." *Elsevier Butterworth Heinmann*, Oxford, UK, 483 pages.
CHANSON, H. (2006). "Air Bubble Entrainment in Hydraulic Jumps. Similitude and Scale Effects." *Report No. CH57/05*, Dept. of Civil Engineering, The University of Queensland, Brisbane, Australia, Jan., 119 pages.
CHANSON, H., and GONZALEZ, C.A. (2005). "Physical Modelling and Scale Effects of Air-Water Flows on Stepped Spillways." *Journal of Zhejiang University SCIENCE*, Vol. 6A, No. 3, March, pp. 243-250).
CHANSON, H., and TOOMBES, L. (1997). "Flow Aeration at Stepped Cascades." *Research Report No. CE155*, Dept. of Civil Engineering, University of Queensland, Australia, June, 110 pages.
CHANSON, H., and TOOMBES, L. (2002). "Air-Water Flows down Stepped chutes : Turbulence and Flow Structure Observations." *Intl Jl of Multiphase Flow*, Vol. 27, No. 11, pp. 1737-1761.
CHANSON, H., and TOOMBES, L. (2004). "Hydraulics of Stepped Chutes: the Transition Flow." *Jl of Hyd. Res.*, IAHR, Vol. 42, No. 1, pp. 43-54.
GONZALEZ, C.A. (2005). "An Experimental Study of Free-Surface Aeration on Embankment Stepped Chutes." *Ph.D. thesis*, Department of Civil Engineering, The University of Queensland, Brisbane, Australia, 240 pages.
HOYT, J.W., and SELLIN, R.H.J. (1989). "Hydraulic Jump as 'Mixing Layer'." *Jl of Hyd. Engrg.*, ASCE, Vol. 115, No. 12, pp. 1607-1614.
OHTSU, I., and YASUDA, Y. (1997). "Characteristics of Flow Conditions on Stepped Channels." *Proc. 27th IAHR Biennial Congress*, San Francisco, USA, Theme D, pp. 583-588.
RAJARATNAM, N. (1990). "Skimming Flow in Stepped Spillways." *Jl of Hyd. Engrg.*, ASCE, Vol. 116, No. 4, pp. 587-591.
RUFF, J.F., and FRIZELL, K.H. (1994). "Air Concentration Measurements in Highly-Turbulent Flow on a Steeply-Sloping Chute." *Proc. Hydraulic Engineering Conf.*, ASCE, Buffalo, USA, Vol. 2, pp. 999-1003.
TOOMBES, L. (2002). "Experimental Study of Air-Water Flow Properties on Low-Gradient Stepped Cascades." *Ph.D. thesis*, Dept of Civil Engineering, The University of Queensland, Brisbane, Australia.